Available online at www.sciencedirect.com
SCIENCE DIRECT®
Journal of Solid State Chemistry 179 (2006) 941–948
JOURNAL OF SOLID STATE CHEMISTRY
www.elsevier.com/locate/jssc

Synthesis and characterization of the pseudo-hexagonal hollandites $A\mathrm{Li_2Ru_6O_{12}}$ (A = Na, K)

M.L. Foo[a,*], T. He[b], Q. Huang[c], H.W. Zandbergen[d], T. Siegrist[e], G. Lawes[f], A.P. Ramirez[e], R.J. Cava[a]

[a]Department of Chemistry, Princeton University, Princeton, NJ, USA
[b]Dupont Central Research and Development, Wilmington, DE, USA
[c]Center for Neutron Research, NIST, Gaithersburg, MD, USA
[d]National Center for High Resolution Electron Microscopy, Delft Institute of Technology, Delft, The Netherlands
[e]Lucent Technologies, Bell Labs, Murray Hill, NJ, USA
[f]Department of Astronomy and Physics, Wayne State University, Detroit, MI, USA

Received 25 September 2005; received in revised form 5 December 2005; accepted 9 December 2005
Available online 20 January 2006

Abstract

The crystal structures, synthesis and physical properties of ruthenium hollandites $A\mathrm{Li_2Ru_6O_{12}}$ (A = Na, K) with a new pseudo-hexagonal structure type are described. Analogous to tetragonal hollandites, the framework is made of $\mathrm{MO_6}$ octahedra in double chains that share corner oxygens with each other to create interstitial tunnels. The tunnels are either hexagonal or triangular in cross-section. Magnetic susceptibilities, low temperature specific heat, and electrical resistivities are reported. The data indicate that these materials are normal, low density of states metals. This new structure type can be extended from A = Group I to A = Group II ions with the synthesis of $\mathrm{CaLi_2Ru_6O_{12}}$ and $\mathrm{SrLi_2Ru_6O_{12}}$.

Keywords: Ruthenates; Hollandites; Pseudo-hexagonal; Neutron diffraction; Electron diffraction; Specific heat; Magnetic susceptibility; Single-crystal X-ray diffraction

1. Introduction

There has been resurgence in research on ruthenates due to the richness of their electrical and magnetic properties [1]. Their electronic behavior can be itinerant or localized, depending on subtle structural or chemical influences. In the Ruddlesden–Popper phases, for example, three-dimensional $\mathrm{SrRuO_3}$ is a rare 4*d* ferromagnet, layered $\mathrm{Sr_2RuO_4}$ is a spin triplet superconductor [2,3], and $\mathrm{Sr_3Ru_2O_7}$, intermediate in dimensionality, is metamagnetic [4]. Doping, either chemically or by pressure, can also tip this precarious balance between ferromagnetism and other exotic electronic states. For example, $\mathrm{CaRuO_3}$ can be tuned from a paramagnetic to a ferromagnetic state through doping of 2% Ti [5]. $\mathrm{Ca_2RuO_4}$, a Mott insulator becomes metallic by doping with 10% Sr [6]. Under applied pressure, $\mathrm{Sr_3Ru_2O_7}$ crosses to a ferromagnetic state from a paramagnetic, strongly correlated Fermi liquid [7].

Besides the three-dimensional perovskites, the one-dimensional hollandite structure type may exhibit interesting physical properties as well. Hollandites have the formula $A_xB_8\mathrm{O_{16}}$ and are typically tetragonal in symmetry [8]. Structurally, they consist of double chains of edge-shared transition metal $\mathrm{BO_6}$ octahedra sharing corners to form large, four-sided tunnels along the *c*-axis in which alkali or alkaline earth cations reside. Hollandites can display variable stoichiometry, i.e., $0.7<x<2.0$ and superlattice ordering among the A cations.

For the alkaline ruthenium hollandites, tetragonal $\mathrm{NaRu_4O_8}$ [9], $\mathrm{KRu_4O_8}$ [10], and $\mathrm{RbRu_4O_8}$ [10] with space

*Corresponding author. Current address: Materials Chemistry Group, The Lash Miller Laboratories, Department of Chemistry, The Faculty of Arts and Sciences, University of Toronto, Ont., Canada M5S 3H6. Fax: +1 416 978 8775.
E-mail address: mfoo@princeton.edu (M.L. Foo).

0022-4596/$ - see front matter © 2005 Elsevier Inc. All rights reserved.
doi:10.1016/j.jssc.2005.12.011

group $I4/m$ are known. The physical characterization of KRu_4O_8, $RbRu_4O_8$, and $Cs_{0.8}Li_{0.2}Ru_4O_8$ has recently been reported [11]. They were found to be metallic paramagnets with conventional transport properties. For $BaRu_6O_{12}$, the only known alkaline earth ruthenium hollandite, an unusual electronic state at low temperature, has been reported [12].

Here we report the synthesis of a new family of pseudo-hexagonal hollandites $MLi_2Ru_6O_{12}$, where $M = Na$, K, Ca, and Sr. Crystal structures and physical properties of $A = Na$ and K are also reported. This new hollandite structure type was initially discovered in the exploration of the Na_2O–Li_2O–RuO_2 phase diagram.

2. Synthesis and characterization

The starting materials used for synthesis of $ALi_2Ru_6O_{12}$ were RuO_2 (Cerac, 99.9%), Li_2CO_3 (Alfa Products, 99%), and either Na_2CO_3 (Mallinckrodt, 99.9%), K_2CO_3 (Alfa Products, 99%), $CaCO_3$ (Baker & Adamson, 99%) or $SrCO_3$ (Aldrich, 99.9%). For $A = Na$, K, and Sr, stoichiometric amounts of RuO_2, Li_2CO_3, and the respective carbonate were mixed and heated at 1100 °C for 16 h in a Zr-gettered nitrogen atmosphere. The powders were placed in dense alumina crucibles that were wired shut to prevent excessive alkali evaporation. For $CaLi_2Ru_6O_{12}$, a mixture of RuO_2 and Ru (Alfa-Aesar 99.999%, 300 mesh) in the molar ratio of 5.5:0.5 was used instead of pure RuO_2. The synthesis of these compounds is extremely sensitive to synthetic conditions. Single crystals of $NaLi_2Ru_6O_{12}$ were obtained from powder synthesis where the starting composition was one molar equivalent of Na, Li, and Ru. A crystal of dimensions $0.20 \times 0.20 \times 0.20$ mm was used for structural solution by single-crystal X-ray diffraction (XRD). Similarly, single crystals of $KLi_2Ru_6O_{12}$ were obtained from powder synthesis using stoichiometric amounts of K, Li, and Ru starting materials. A crystal of dimensions $0.02 \times 0.02 \times 0.20$ mm was used for structural solution by single-crystal XRD of this variant.

All samples were characterized by X-ray powder diffraction using Cu$K\alpha$ radiation. Temperature-dependent magnetic susceptibility measurements of $NaLi_2Ru_6O_{12}$ and $KLi_2Ru_6O_{12}$ were collected using a Quantum Design PPMS in a DC field of 1 T on zero field cooling. Resistivity and specific heat measurements were performed on sintered pellets of $NaLi_2Ru_6O_{12}$ using the standard four-lead AC technique and a Quantum Design PPMS, respectively. The pellets were obtained by pressing the polycrystalline powder into a $\frac{1}{4}''$ pellet, followed by sintering at 1100 °C in nitrogen for 4 h. Single-crystal XRD of $NaLi_2Ru_6O_{12}$ and $KLi_2Ru_6O_{12}$ was performed using a Bruker Smart and an Oxford-Diffraction Xcalibur 2 diffractometer.

Neutron powder diffraction intensity data was collected using the BT-1 high-resolution powder diffractometer at the NIST Center for Neutron Research, employing a Cu (311) monochromator to produce a neutron beam of wavelength 1.5403 Å. Collimators with horizontal divergences of 15′, 20′, and 7′ of arc were used before and after the monochromator, and after the sample, respectively. The intensities were measured in steps of 0.05° in the 2θ range 3–168°. The structural parameters were refined using the program GSAS [13]. The neutron scattering amplitudes used in the refinements were 0.363, −0.203, 0.721, and 0.581 ($\times 10^{-12}$ cm) for Na, Li, Ru, and O, respectively. Electron microscopy analysis was performed with Philips CM300UT electron microscope having a field emission gun and operated at 300 kV.

Table 1
Atomic positions and thermal parameters for $NaLi_2Ru_6O_{12}$ determined by single-crystal XRD

	Pos.	x	y	z	B_{iso}	Occ.
Ru	6*h*	0.36035(24)	0.01829(25)	1/4	0.60(11)	
O1	6*h*	0.4603(20)	0.8648(20)	1/4	0.3(3)	
O2	6*h*	0.2953(19)	0.1937(20)	1/4	0.2(3)	
Na	2*a*	0	0	1/4	4.0(4)	1/3
Li	2*d*	2/3	1/3	1/4	0.5(13)	
	$u_{11}(U)$	u_{22}	u_{33}	u_{12}	u_{13}	u_{23}
Ru	0.66(11)	0.69(13)	0.89(12)	0.31(9)	0.0	0.0
O1	0.4(4)					
O2	0.2(4)					
Na	0.3(11)	0.3	14.0(9)	0.2	0.0	0.0
Li	0.7(16)					

B_{iso} is the mean of the principal axes of the thermal ellipsoid.
Space group $P6_3/m$ (No. 176), $a = 9.3762(13)$ Å, $c = 2.7786(6)$ Å, and $V = 211.14(5)$ Å^3 (pseudo-hexagonal symmetry subcell).
Note: Occupancy of the Na site is not well defined in these refinements, it is estimated at 1/3 and fixed.
Table of $u(i,j)$ or U values × 100.
The last least-squares cycle was calculated with five atoms, 16 parameters, and 113 of 125 reflections. For significant reflections, $R_F = 0.044$, $R_w = 0.051$. For all reflections, $R_F = 0.044$, $R_w = 0.051$.

3. Discussion

From structural refinement of the single-crystal XRD data for $NaLi_2Ru_6O_{12}$ (Table 1) and $KLi_2Ru_6O_{12}$ (Table 2), a new hollandite structure type common to both compounds was identified. For both materials, the space group $P6_3/m$ (176) was found to well describe the diffraction data, with cell parameters, for $NaLi_2Ru_6O_{12}$, of $a = 9.3762(13)$ Å, $c = 2.7786(6)$ Å; and for $KLi_2Ru_6O_{12}$, $a = 9.4053(9)$ Å, $c = 2.7672(4)$ Å. A weak superstructure of $2a$, $2b$, and $2c$ seen in both the Na and K hollandites was not included in the refinement. The structure can be described as a hexagonal hollandite (Fig. 1), which has double chains of edge-sharing RuO_6 octahedra interconnected by corner sharing to form a three-dimensional framework with channels that accommodate the alkali/alkaline earth cations. Two types of channels are present, triangular and hexagonal. The alkali/alkaline earth ions reside in the hexagonal channels where their positions are disordered. The triangular channels are occupied by Li ions that are in trigonal prismatic coordination. Nonstoichiometry in the hexagonal tunnels is indicated, but definite conclusions about this cannot be drawn from the X-ray refinement due to the relatively small contributions of the alkalis to the diffracted intensities, the high apparent temperature factors for the alkali atoms, and the complex structural distortions observed in the neutron diffraction data (see below). The structure of the ruthenium oxide framework is similar to the mineral fluoborite, $Mg_3((F,OH)_3BO_3)$ [14]. In fluoborite, the structure consists of a framework of MgO_6 octahedra with triangular channels occupied by boron. Due to the presence of F and OH, there are no cations present in the hexagonal channels. Other minerals related to fluoborite include paninite $CaZrB(Al_9O_{18})$ [15] and jeremevite $B_5(Al_6(OH)_3O_{15})$ [16]. All three minerals have the same space group as this new hexagonal ruthenium hollandite.

Table 2
Atomic positions and thermal parameters for $KLi_2Ru_6O_{12}$ determined by single-crystal XRD

	Pos.	x	y	z	B_{iso}	Occ.
Ru	6*h*	0.35994(20)	0.01736(22)	1/4	0.99(9)	
O1	6*h*	0.4585(20)	0.8638(24)	1/4	2.4(11)	
O2	6*h*	0.2962(20)	0.1932(20)	1/4	1.6(9)	
K	2*a*	0	0	1/4	13.0(45)	1/3
Li	2*d*	2/3	1/3	1/4	0.5(6)	
	$u_{11}(U)$	u_{22}	u_{33}	u_{12}	u_{13}	u_{23}
Ru	0.72(9)	1.10(10)	1.97(9)	0.48(8)	0.0	0.0
O1	2.8(10)	6.4(14)	1.9(10)	3.8(10)	0.0	0.0
O2	3.7(10)	3.0(10)	1.2(8)	3.2(9)	0.0	0.0
K	3.0(1)	3.0(0)	44.0(98)	1.0(0)	0.0	0.0
Li	0.6(8)				0.0	0.0

B_{iso} is the mean of the principal axes of the thermal ellipsoid.
Space group: $P6_3/m$ (No. 176), $a = 9.4053(9)$Å, $c = 2.7672(4)$ Å, and $V = 211.99(4)$ Å^3 (pseudo-hexagonal symmetry subcell).
Note: Occupancy of the *K* site is not well defined in these refinements, it is estimated at 1/3 and fixed.
Table of $u(i,j)$ or U values × 100. The last least-squares cycle was calculated with five atoms, 25 parameters, and 289 out of 304 reflections. For significant reflections, $R_F = 0.087$, $R_w = 0.058$. For all reflections, $R_F = 0.106$, $R_w = 0.095$.

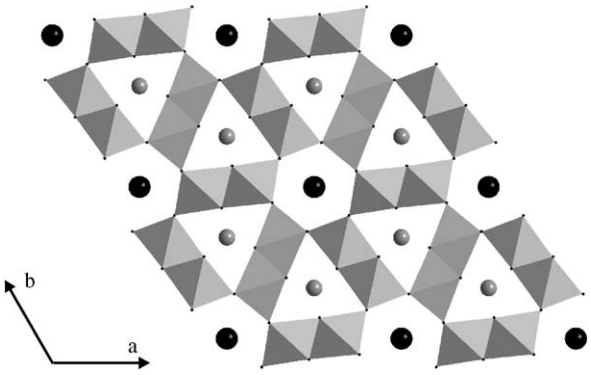

Fig. 1. The crystal structure of $NaLi_2Ru_6O_{12}$ with emphasis on RuO_6 coordination polyhedra. Hexagonal subcell space group $P6_3/m$. Gray spheres represent Li; black spheres, Na.

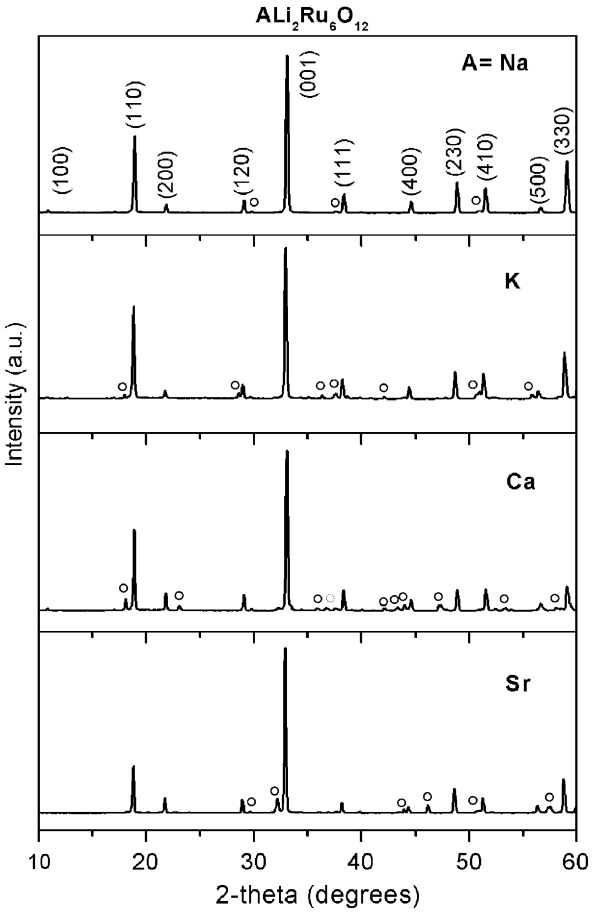

Fig. 2. Low-angle powder XRD patterns (Cu$K\alpha$) of (a) $NaLi_2Ru_6O_{12}$, (b) $KLi_2Ru_6O_{12}$, (c) $CaLi_2Ru_6O_{12}$, and (d) $SrLi_2Ru_6O_{12}$. The peaks for $NaLi_2Ru_6O_{12}$ are indexed to a hexagonal symmetry cell. Open circles represent impurity phases.

The low-angle powder XRD patterns of $NaLi_2Ru_6O_{12}$, $KLi_2Ru_6O_{12}$, $CaLi_2Ru_6O_{12}$, and $SrLi_2Ru_6O_{12}$ are shown in Fig. 2. The patterns can be indexed on a hexagonal cell consistent with the results obtained from single-crystal XRD. Their lattice parameters are given in Table 3. It is observed that there is a minor unidentifiable phase common in all the powder patterns. For $A = K$, there are additional unidentifiable phase(s). For $A = Sr$, $SrRuO_3$ could be identified as an impurity. For $A = Ca$, $CaRuO_3$ perovskite and Ru are impurities. Phase purity was extremely difficult to achieve, especially for $A = K$, Sr, and Ca. Further work would be required to optimize synthetic conditions.

Table 3
Lattice parameters of synthesized $ALi_2Ru_6O_{12}$ hollandites obtained by X-ray refinement of single crystals, $A = Na$, K, and polycrystalline samples, $A = Ca$, Sr (pseudo-hexagonal symmetry subcell).

	a (Å)	c (Å)
$NaLi_2Ru_6O_{12}$	9.3672(13)	2.7786(6)
$KLi_2Ru_6O_{12}$	9.4053(9)	2.7672(4)
$CaLi_2Ru_6O_{12}$	9.363(2)	2.697(1)
$SrLi_2Ru_6O_{12}$	9.412(2)	2.721(2)

On analysis of the high-resolution neutron powder diffraction pattern of $NaLi_2Ru_6O_{12}$ at 295 K (Fig. 3), it was found that the structure could not be satisfactorily refined with hexagonal symmetry. Although a partial fit could be obtained with a hexagonal cell of $a = 9.375$ Å and $c = 2.78$ Å, reflections with $l \neq 0$ are split: for example, the hexagonal reflections (321) and (411) are split into at least two peaks (Fig. 3a). These peaks would not be split in hexagonal symmetry. One reason for this splitting might be the presence of two phases with different c-axis; however the (002) reflection, shown in the inset of Fig. 3, is a single

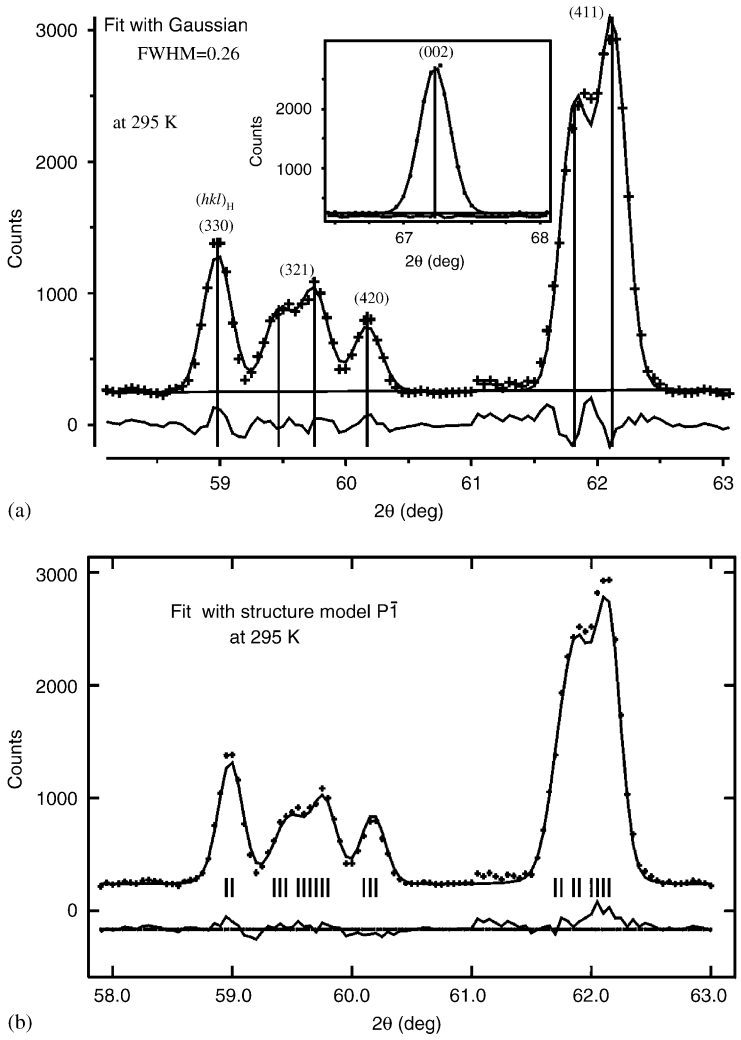

Fig. 3. Selected portion of neutron powder diffraction pattern for $NaLi_2Ru_6O_{12}$ at 295 K. (a) Gaussian fit gives a full-width at half-maximum (FWHM) of 0.26° (the instrumental resolution). The Miller indices of the peaks shown in the figure would correspond to a hexagonal unit cell. Reflections with those having $l \neq 0$ are split; reflections such as (321) and (411), for example, are split into at least two peaks. The inset shows that the (002) reflection is a single peak, indicating that the splitting of (321) and (411) cannot be due to two phases with different hexagonal c-axis. (b) A good fit was obtained with triclinic symmetry $P\bar{1}$ for $NaLi_2Ru_6O_{12}$.

Table 4
Atomic and lattice parameters of the triclinic symmetry subcell of $NaLi_2Ru_6O_{12}$ determined by neutron diffraction at 295 and 15 K

	Frac.	x	y	z	$100 \times U_{iso}$ (Å^2)
295 K					
$a = 9.3767(5)$ Å, $b = 9.3843(4)$ Å, $c = 2.7806(1)$ Å, $\alpha = 90.402(2)^\circ$, $\beta = 89.875(4)^\circ$, $\gamma = 120.001(5)^\circ$. Cell volume, $V = 211.89(2)$ Å^3					
Na	1.000	0.0000	0.0000	0.0000	12.2(1.0)
Li		0.3333	0.6667	0.2500	7.9(6)
Ru1		0.6395(3)	0.9828(3)	0.2500	1.36(4)
Ru2		−0.9828(3)	−0.3422(3)	0.2500	1.36(3)
Ru3		0.3422(3)	−0.6394(3)	0.2500	1.36(3)
O1		0.4589(4)	0.8667(3)	0.7500	0.94(3)
O2		0.7076(4)	0.8075(3)	0.2500	0.94(3)
O3		−0.8667(3)	−0.4041(4)	0.7500	0.94(3)
O4		0.4041(4)	−0.4589(4)	0.7500	0.94(3)
O5		−0.8075(3)	−0.1059(4)	0.2500	0.94(3)
O6		0.1059(4)	−0.7076(4)	0.2500	0.94(3)
15 K					
$a = 9.3692(6)$ Å, $b = 9.3747(3)$ Å, $c = 2.7757(1)$ Å, $\alpha = 90.448(2)^\circ$, $\beta = 89.781(3)^\circ$, $\gamma = 120.017(4)^\circ$. Cell volume, $V = 211.09(2)$ Å^3					
Na	1.000	0.0000	0.0000	0.000	8.7(6)
Li		0.3333	0.6667	0.250	6.8(5)
Ru1		0.6384(7)	0.9831(9)	0.270(2)	1.03(4)
Ru2		−0.9820(8)	−0.3402(8)	0.250(2)	1.03(4)
Ru3		0.3410(8)	−0.6423(9)	0.259(2)	1.03(4)
O1		0.4648(9)	0.8665(10)	0.754(2)	0.61(3)
O2		0.7026(10)	0.8113(9)	0.255(2)	0.61(3)
O3		−0.8675(11)	−0.4076(11)	0.754(2)	0.61(3)
O4		0.4071(8)	−0.4563(10)	0.763(2)	0.61(3)
O5		−0.8151(9)	−0.1058(10)	0.255(2)	0.61(3)
O6		0.0988(8)	−0.7018(9)	0.252(2)	0.61(3)

Space group: $P\bar{1}$ (No. 2). Na atoms are in the 1*a* (000) site and all the other atoms are in the 2*i* (*xyz*) site.
$R_p = 5.80\%$, $R_{wp} = 7.19\%$, $\chi^2 = 2.389$ for 32 variables.
$R_p = 5.63\%$, $R_{wp} = 7.308\%$, $\chi^2 = 3.009$ for 57 variables.

peak, excluding this possibility. This implies that the structure has a lower symmetry than hexagonal. Orthorhombic and monoclinic symmetry cells were found to be inadequate for indexing the pattern: a triclinic symmetry cell with $a = 9.3767(5)$ Å, $b = 9.3843(4)$ Å, and $c = 2.7806(1)$ Å, and $\alpha = 90.402(2)^\circ$, $\beta = 89.875(4)^\circ$, and $\gamma = 120.001(5)^\circ$ was found to be necessary (Fig. 3b) to yield a good fit. The atomic and lattice parameters of $NaLi_2Ru_6O_{12}$ for 295 and 15 K refined with space group $P\bar{1}$ (No. 2) are shown in Table 4. No significant structural distortions were observed to develop between 295 and 15 K, and at 15 K, fewer constraints need to be applied in the structural refinement due to the reduction of thermal vibrations. The lattice parameters and angles of the triclinic cell are very close to those of a hexagonal cell, though they are many standard deviations different from the hexagonal values, and thus the structure is pseudo-hexagonal. The ruthenium oxide framework has essentially hexagonal symmetry, and we speculate that the single crystals appear to have hexagonal symmetry due to the presence of nanometer scale twinning (see below).

From single-crystal XRD and transmission electron microscopy experiments, a superlattice structure for $NaLi_2Ru_6O_{12}$ is indicated. Electron diffraction was performed on a specimen prepared in the same way as the one that was used for the neutron diffraction experiments. The electron diffraction showed extra reflections in the $0\,0\,l$ planes with $l = n + \frac{1}{2}$, indicating a doubling of the *c*-axis. Using electron nanodiffraction, it was determined that the superstructure is a, $a\sqrt{3}$, and $2c$ with an I centering. Very strong twinning was observed, even on the very short 10 nm length scale (Fig. 4). Taking into account the twinning, the observed superstructure is in agreement with the single-crystal XRD results, in which a $2a$, $2b$, and $2c$ superstructure was observed.

The relationships between sublattice and superlattice are shown in Fig. 5, $a_{sup} = a_{sub}$, $b_{sup} = \sqrt{3}b_{sub}$, $c_{sup} = 2c_{sub}$, $\alpha_{sup} = \alpha_{sub}$, $\beta_{sup} = \beta_{sub}$, and $\gamma_{sup} = \gamma_{sub} - 30$, where the structure parameters for the sublattice are shown in Table 4. The refinement was performed with I symmetry, which is an unconventional choice of triclinic cell, but taken because it facilitates an easier comparison to the higher symmetry hexagonal subcell. Refinement was only performed in $I\bar{1}$ and not $I1$ because there are 252 independent atomic coordinates to be refined in the latter (and 126 for $I\bar{1}$). Refinement with a superstructure in $I\bar{1}$ gave an improved indexing to the observed Bragg peaks, as shown in Fig. 6, in which the superpeaks (103) and (−1,0,3) are seen. The goodness-of-fit parameter χ^2 reduced from 2.389 and 3.009 (Table 4) to 1.390 and 1.658 (Table 5) at 295 and 15 K, respectively, when the superlattice was included. The results are shown in Table 5. The portion of the calculated and observed neutron powder diffraction intensity pattern at 295 K in Fig. 6 indicates that the calculated intensities of the superlattice peaks (103) and (−1, 0, 3) give a good fit to the observed intensities of the peak at 2θ–50°.

For refinements in both the triclinic subcell and supercell structural models, when allowed to refine as a free parameter, the Na site was found to be fully occupied, yielding a stoichiometry $NaLi_2Ru_6O_{12}$. One possible explanation for the doubling of the *c*-axis in the supercell, however (the direction perpendicular to the plane shown in Fig. 1), could be a short-range empty–full–empty–full ordering of the Na atoms along the hexagonal tunnel. Such an ordering would increase the Na–Na separation in the tunnels and would also explain the doubling along *b* if the Na occupancy in adjacent tunnels is "out of phase", yielding a stoichiometry $Na_{0.5}Li_2Ru_6O_{12}$. When the Na site is constrained to have an occupancy fixed at 0.5, the agreement is clearly worse than for the case where the site is completely filled ($\chi^2 = 1.49$ as opposed to 1.39, in the supercell model), with a substantially smaller Na temperature factor (B_{iso} of 1.1 vs 5.7). Whereas these refinements favor a full Na site occupancy, the X-ray single-crystal refinements suggest $\frac{2}{3}$ occupancy. Since large-atom ordering in tunnels in the tetragonal hollandites often leads to incommensurate periodicities, short-range order, and nonstiochiometric tunnel occupancy, it would not be

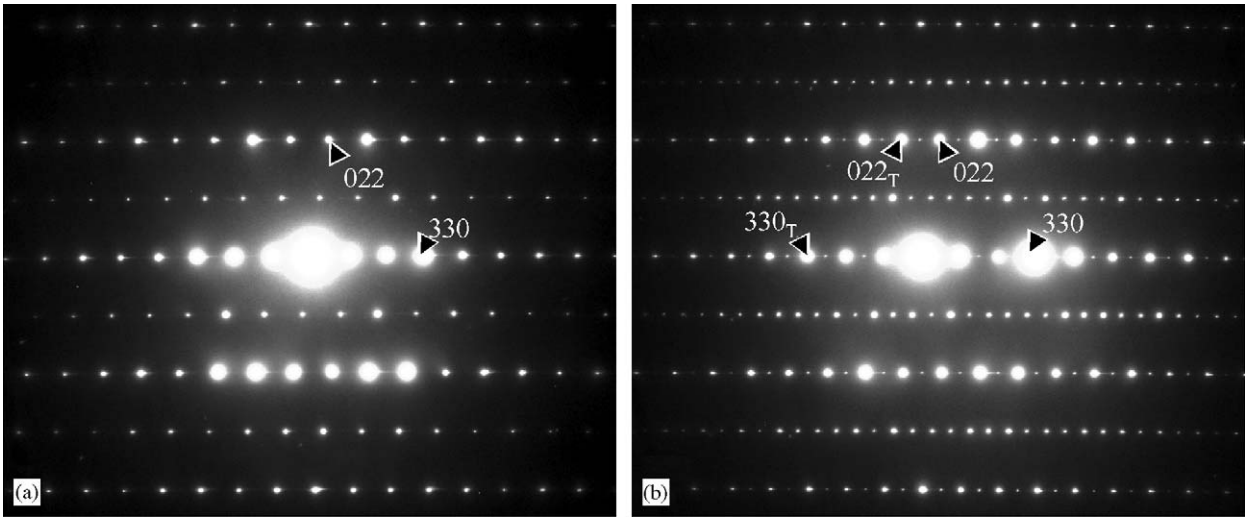

Fig. 4. Electron nanodiffraction (10 nm spot) patterns of $NaLi_2Ru_6O_{12}$. (a) and (b) show [1 $\bar{1}$ 1] electron diffraction patterns without and with twinning, respectively. (b) The sum of the diffraction pattern in (a) and the twin related by a mirror (vertical mirror plane). The indexing refers to the supercell with the doubled *c*-axis. Twinned spots are labeled with a T subscript.

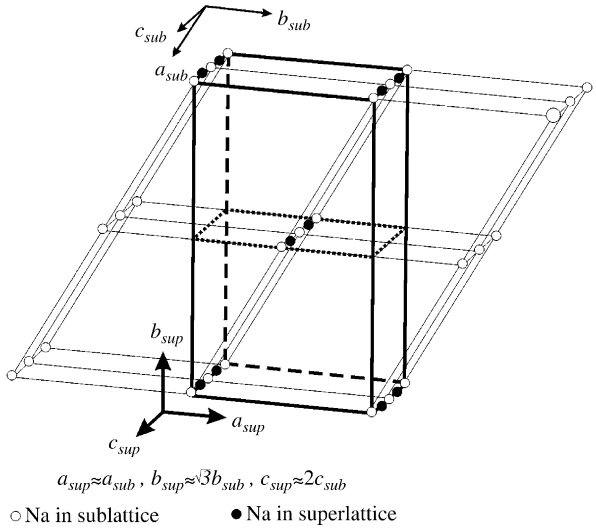

Fig. 5. The relationships between sublattice and superlattice: $a_{sup} = a_{sub}$, $b_{sup} = \sqrt{3}b_{sub}$, $c_{sup} = 2c_{sub}$, $\alpha_{sup} = \alpha_{sub}$, $\beta_{sup} = \beta_{sub}$, and $\gamma_{sup} = \gamma_{sub} - 30$, where the structure parameters for the sublattice are shown in Table 4. Solid circles present the lattice points of the sublattice, suggesting that the superstructure has a *C*- or *I*-centered lattice with a center symmetry.

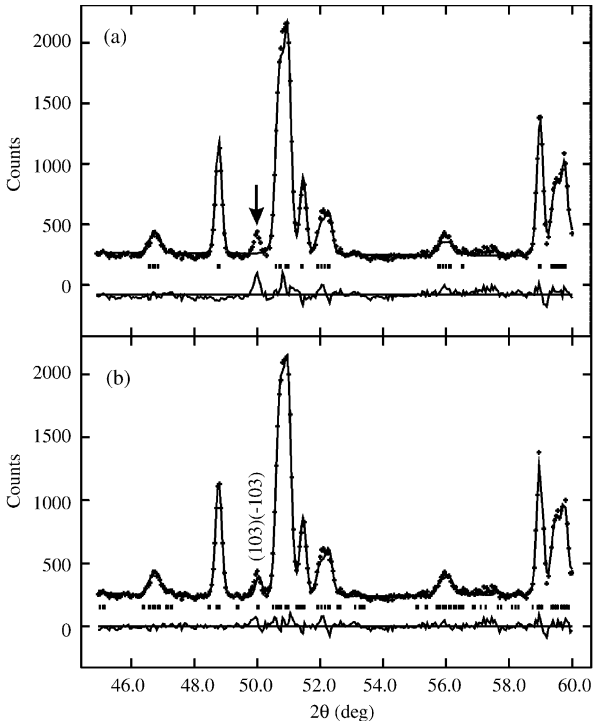

Fig. 6. Portion of the calculated and observed neutron powder diffraction intensity pattern for at 295 K. (a) Fit by a substructure model with structure parameters shown in Table 4 where there are not calculated Bragg peaks for the observed peak at 2θ–50°. (b) Fit by a superstructure model with structure parameters shown in Table 5 showing the superlattice peaks (103) and (−1, 0, 3) give a good fit to the observed intensities of the peak at 2θ–50°.

unexpected for the true Na content in the tunnels in the current compound to deviate from 1. We conclude that the quality of the current data is not sufficient for a full specification of the Na positions and occupancies. More detailed study would be required to clarify this issue. The Li site occupancy in the small tunnel was found to be stoichiometric.

The magnetic susceptibilities of $NaLi_2Ru_6O_{12}$ and $KLi_2Ru_6O_{12}$ are shown in Fig. 7. Their susceptibility behavior reveals that these compounds are Pauli paramagnetic with χ_0 of $\sim 10^{-4}$ emu/Oe mol Ru. This lack of Ru local moment is similar to what is observed in the tetragonal Ru hollandites such as KRu_4O_8 [11]. For $CaLi_2Ru_6O_{12}$ and $SrLi_2Ru_6O_{12}$, no meaningful magnetic data could be obtained because in each case there was strong interference from the contributions of $CaRuO_3$ and $SrRuO_3$ impurities, respectively. Temperature-dependent resistivity measurements (Fig. 7, inset) on a

Table 5
Results obtained from refinements with a superlattice structure having $I\bar{1}$ symmetry for $NaLi_2Ru_6O_{12}$ at 295 and 15 K

Name	x	y (000) +	z (1/2, 1/2, 1/2) +	$U_{iso} \times 100$ (Å^2)
295 K				
$a = 9.3771(5)$ Å, $b = 16.2533(8)$ Å, $c = 5.5615(2)$ Å, $\alpha = 90.393(2)^\circ$, $\beta = 89.859(5)^\circ$, $\gamma = 90.023(6)^\circ$. Cell volume, $V = 847.57(7)$ Å^3				
Na	0.004(8)	−0.0059(25)	0.308(4)	7.0(7)
Li1	0.0311(21)	0.3260(19)	0.3251(31)	1.82
Li2	0.0311(21)	0.3260(19)	0.8701(31)	1.82
Ru1	0.1618(12)	0.1807(7)	0.3604(15)	0.64(4)
Ru2	0.1626(13)	0.1804(7)	0.8897(15)	0.64(4)
Ru3	0.3533(12)	0.0087(7)	0.1404(17)	0.64(4)
Ru4	0.3476(11)	0.0091(7)	0.6072(16)	0.64(4)
Ru5	0.3149(12)	0.6678(7)	0.1483(15)	0.64(4)
Ru6	0.3090(12)	0.6739(8)	0.6069(15)	0.64(4)
O1	0.8293(16)	0.2998(9)	0.1181(17)	0.626(30)
O2	0.8361(16)	0.2955(9)	0.6270(16)	0.626(30)
O3	0.2617(14)	0.5541(9)	0.1251(18)	0.626(30)
O4	0.2530(15)	0.5496(9)	0.6207(18)	0.626(30)
O5	0.0343(14)	0.8565(8)	0.1187(19)	0.626(30)
O6	0.0500(15)	0.8486(9)	0.6325(18)	0.626(30)
O7	0.6949(18)	0.5964(8)	0.1193(19)	0.626(30)
O8	0.7067(15)	0.5944(9)	0.6293(19)	0.626(30)
O9	0.1315(14)	0.2625(8)	0.1305(17)	0.626(30)
O10	0.1375(15)	0.2745(8)	0.6262(18)	0.626(30)
O11	0.0215(16)	0.4313(7)	0.1101(19)	0.626(30)
O12	0.0325(17)	0.4315(9)	0.6302(19)	0.626(30)
15 K				
$a = 9.3665(4)$ Å, $b = 16.2324(7)$ Å, $c = 5.5501(2)$ Å, $\alpha = 90.436(2)^\circ$, $\beta = 89.869(4)^\circ$, $\gamma = 90.025(5)^\circ$, $V = 843.81(6)$ Å^3				
Na	−0.007(5)	−0.0082(18)	0.2925(32)	5.6(6)
Li1	0.001(6)	0.3289(31)	0.336(6)	5.2(5)
Li2	0.001(6)	0.3289(31)	0.881(6)	5.2(5)
Ru1	0.1582(10)	0.1808(6)	0.3597(13)	0.39(4)
Ru2	0.1652(11)	0.1784(6)	0.8954(12)	0.39(4)
Ru3	0.3564(10)	0.0081(7)	0.1426(15)	0.39(4)
Ru4	0.3473(9)	0.0105(6)	0.6064(14)	0.39(4)
Ru5	0.3131(11)	0.6668(6)	0.1401(13)	0.39(4)
Ru6	0.3119(11)	0.6740(6)	0.6115(13)	0.39(4)
O1	0.8278(12)	0.3004(7)	0.1160(14)	0.382(26)
O2	0.8427(12)	0.2943(7)	0.6316(14)	0.382(26)
O3	0.2641(11)	0.5548(7)	0.1280(15)	0.382(26)
O4	0.2501(12)	0.5500(8)	0.6183(15)	0.382(26)
O5	0.0392(12)	0.8568(7)	0.1229(16)	0.382(26)
O6	0.0533(12)	0.8480(7)	0.6283(16)	0.382(26)
O7	0.6996(14)	0.5967(7)	0.1182(16)	0.382(26)
O8	0.7060(13)	0.5932(7)	0.6261(16)	0.382(26)
O9	0.1363(13)	0.2629(7)	0.1288(15)	0.382(26)
O10	0.1375(12)	0.2722(7)	0.6316(16)	0.382(26)
O11	0.0230(14)	0.4319(7)	0.1113(16)	0.382(26)
O12	0.0326(14)	0.4317(7)	0.6312(16)	0.382(26)

Atomic positions shown in this table were constrained to be in a body-centered lattice to reduce the number of variables.
$R_p = 4.49\%$, $R_{wp} = 5.47\%$, $\chi^2 = 1.390$.
$R_p = 4.40\%$, $R_{wp} = 5.48\%$, $\chi^2 = 1.658$.

sintered pellet of $NaLi_2Ru_6O_{12}$ demonstrate poor metallic behavior. Since three-dimensional ruthenium perovskites are generally good metals, this suggests that the Ru–O bonding angles have a significant effect on resistivity. The Ru–O–Ru bond angle in perovskites is around 180°, allowing effective overlap of the Ru and O atomic orbitals, whereas that of $NaLi_2Ru_6O_{12}$ is nearly 130°.

Specific heat measurements (Fig. 8) on sintered pellets of $NaLi_2Ru_6O_{12}$ show that the Sommerfeld parameter γ, which is the electronic contribution to the specific heat, is given by $\gamma = 3.75\,\text{mJ/mol Ru K}^2$. This indicates that the carrier mass is not significantly enhanced, and is very small compared to that of a correlated system such as Sr_2RuO_4 [17], where 40 mJ/mol Ru K^2 is found. There is a change in slope in C/T vs T^2 at around 5 K; however, the cause for

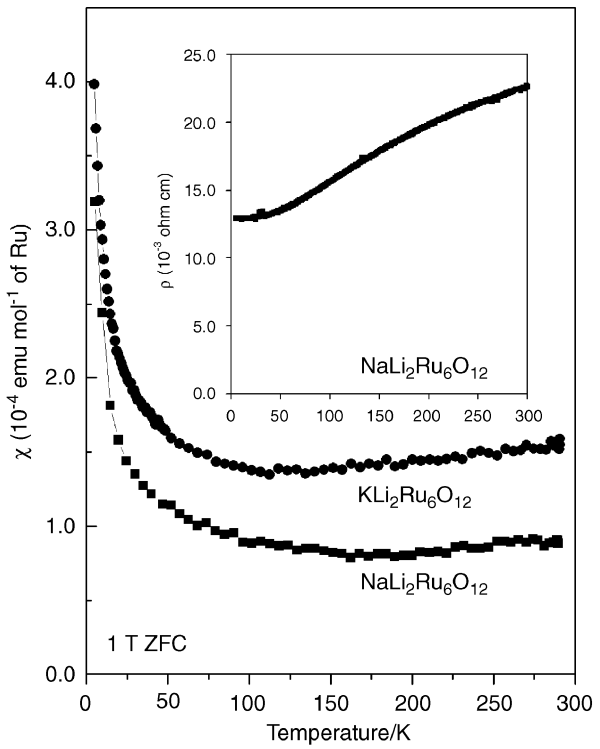

Fig. 7. Temperature-dependent magnetic susceptibility measurements for polycrystalline powders of $NaLi_2Ru_6O_{12}$ and $KLi_2Ru_6O_{12}$ at 1 T on zero field cooling. (Inset) Resistivity vs temperature for a sintered pellet of $NaLi_2Ru_6O_{12}$.

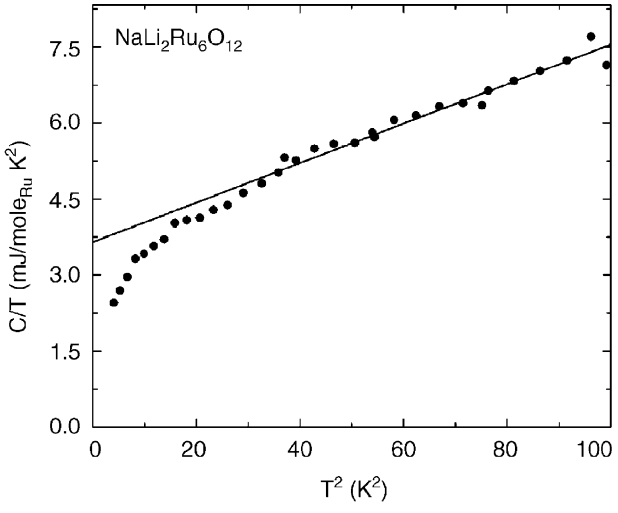

Fig. 8. Temperature-dependent specific heat measurement for a sintered pellet of $NaLi_2Ru_6O_{12}$.

this is presently unknown. No transition is observed at this temperature in the resistivity or magnetic data.

In conclusion, we have synthesized a new ruthenium hollandite structure type that exhibits pseudo-hexagonal instead of tetragonal symmetry. The structure exhibits superlattice ordering and a body-centered triclinic supercell is proposed. In contrast to the tetragonal hollandites, there are two distinct structural tunnels and the arrangement of the RuO_6 octahedra is markedly different. Magnetic susceptibility measurements reveal Pauli paramagnetism for $NaLi_2Ru_6O_{12}$ and $KLi_2Ru_6O_{12}$. Conductivity and specific heat measurements on $NaLi_2Ru_6O_{12}$ indicate poor metallic behavior. Hence, the physical properties exhibited by the pseudo-hexagonal ruthenium hollandites are very similar to that of the tetragonal ruthenium hollandites. The distortion of the structure from simple hexagonal symmetry to triclinic symmetry is surprising, but symmetry lowering is also sometimes observed in "tetragonal" hollandites [18]. For ruthenates, such distortions can often be attributed to coupling between the electronic system and the crystal structure [19,20], suggesting that the electronic state in $NaLi_2Ru_6O_{12}$ may be worthy of further study.

Acknowledgments

This work was supported by the National Science Foundation Solid State Chemistry program, Grant DMR-0244254.

References

[1] R.J. Cava, Dalton Trans. 9 (2004) 2979–2987.
[2] Y. Maeno, H. Hashimoto, K. Yoshida, S. Nishizaki, T. Fujita, J.G. Bednorz, F. Lichtenberg, Nature 372 (1994) 532–534.
[3] Y. Maeno, T.M. Rice, M. Sigrist, Phys. Today 54 (1) (2002) 42–50.
[4] S.A. Grigera, R.S. Perry, A.J. Schofield, M. Chiao, S.R. Julian, G.G. Lonzarich, S.I. Ikeda, Y. Maeno, A.J. Millis, A.P. Mackenzie, Science 294 (2001) 329–332.
[5] T. He, R.J. Cava, J. Phys.: Condens. Mat. 13 (2001) 8347–8361.
[6] O. Freidt, M. Braden, G. Andre, P. Adelmann, S. Nakatsuji, Y. Maeno, Phys. Rev. B 63 (2001) 174432.
[7] S.I. Ikeda, N. Shirakawa, S. Koiwai, A. Uchida, M. Kosaka, Y. Uwatoko, Physica C 364–365 (2001) 376–378.
[8] J.M. Loezos, T.A. Vanderah, A.R. Drews, Powder Diffr. 14 (1999) 31–35.
[9] B.V. Lazarev, L.S. Shapolygin, Russ. J. Inorg. Chem. 25 (1980) 1837–1840.
[10] V. Wilhem, R. Hoppe, Z. Anorg. Allg. Chem. 438 (1978) 90–96.
[11] M.L. Foo, W. Lee, T. Siegrist, G. Lawes, A.P. Ramirez, N.P. Ong, R.J. Cava, Mater. Res. Bull. 39 (11) (2004) 1663–1670.
[12] Z.Q. Mao, T. He, M.M. Rosario, K.D. Nelson, D. Okuno, B. Ueland, I.G. Deac, P. Schiffer, Y. Liu, R.J. Cava, Phys. Rev. Lett. 90 (18) (2003) 186601–186604.
[13] A. Larson, R.B. Von Dreele, Internal Report, Los Alamos National Laboratory, 1994.
[14] Y. Takéuchi, Acta Crystallogr. 3 (1950) 208–210.
[15] T. Armbruster, N. Dobelin, A. Peretti, D. Gunther, E. Reusser, B. Grobety, Am. Mineral. 89 (2004) 610–613.
[16] C. Rodellas, S. Garcia-Blanoc, A. Vegas, Z. Kristallogr. 165 (1983) 225–260.
[17] S. Nishizaki, Y. Maeno, S. Farner, S. Ikeda, T. Fujita, Physica C 282–287 (1997) 1413–1414.
[18] M.L. Carter, Mater. Res. Bull. 39 (2004) 1075–1081.
[19] Y. Yoshida, S.I. Ikeda, H. Matsuhata, N. Shirakawa, C.H. Lee, S. Katano, Phys. Rev. B 72 (2005) 054412.
[20] P. Khalifah, R. Osborn, Q. Huang, H.W. Zandbergen, R. Jin, Y. Liu, D. Mandras, R.J. Cava, Science 297 (2002) 2237–2240.